

Study and explanation about the morphological, electrochemical and structural properties of differently synthesized polypyrrole

Shruti Peshoria¹ · Anudeep Kumar Narula¹

Received: 19 June 2017 / Accepted: 20 August 2017 / Published online: 9 September 2017
© Springer Science+Business Media, LLC 2017

Abstract Polypyrrole (ppy), a conducting polymer was synthesized by four different polymerization methods viz. electrochemical polymerization (EP), interfacial polymerization (IP), chemical oxidative polymerization (COP) and template-assisted polymerization (TAP). The change in morphology that occurred due to the variation of polymerization method used was studied with scanning electron microscopy (SEM) and high-resolution transmission electron microscopy (HRTEM). The samples were analyzed by Fourier transform infrared (FT-IR) spectroscopy to confirm the successful polymerization of pyrrole to polypyrrole with the appearance of characteristic bands for N–H stretching, C–N stretching, ppy ring stretching, C–H and C–C bending vibrations. Optical studies were done by UV–Vis absorption spectroscopy that displayed $\pi \rightarrow \pi^*$ and polaronic/bipolaronic transitions of ppy. XRD analysis revealed amorphous nature of ppy. Examination of SEM micrographs disclosed that ppy synthesized by EP had the typical cauliflower structure while ppy formed by IP were in the form of chain like network with a thickness of 250–290 nm, COP resulted in the formation of interlinked microspheres of polypyrrole and TAP formed polypyrrole nanofibers. Electrochemical characterization showed that ppy prepared by EP had the lowest redox activity and the samples were also tested to detect Pb^{2+} .

1 Introduction

The discovery of conductive polyacetylene in 1977 [1] led to the beginning of extensive research into the field of conducting polymers. Conducting polymers also known as synthetic metals [2] combine the advantages of polymeric materials like flexibility, light weight, low density, corrosion resistance, easy manufacturing, low finishing costs, toughness and ductility with those of metals that are electrically conducting, thus making possible the development of lightweight electronics in any desirable shape with ease of manufacturing and corrosion resistance. Conducting polymers like polypyrrole, polyaniline, poly(3,4-ethylene dioxithiophene) and various polythiophene derivatives are the new and capable candidates to be used in sensors [3–5], electrocatalysts [6], supercapacitors [7, 8] and dye sensitized solar cells (DSSCs) [9, 10] due to their high conductivity, environmental stability, cost effectiveness and electrochemical redox properties. Among these, polypyrrole is one of the most extensively studied conducting polymers as, in addition to above advantages it is biocompatible, thermally stable, has high polymerization yield, charge storage capacity and surface area [11–14]. Applicability of polypyrrole as a functional material depends strongly on its morphology as properties like surface area [15], conductivity [16], thermal stability and optical band gap are determined by its size and structure [17]. Usefulness of polypyrrole in the reported literature, as antibacterial agent [18], catalyst [19, 20], pH sensor [21], supercapacitor [22–24], thermoelectric material [25], counter electrode in dye-sensitized solar cells [26], photothermal agent in photothermal therapy [27] and biosensor [28] also suggest the role of morphology. Furthermore, morphology of ppy is dependent on the preparation technique and reaction conditions used [29, 30].

✉ Anudeep Kumar Narula
researchchemlab58@gmail.com

Shruti Peshoria
shrutipeshoria@gmail.com

¹ Molecular Chemistry Laboratory, University School of Basic and Applied Sciences, Guru Gobind Singh Indraprastha University, Sector-16 C, Dwarka, New Delhi 110078, India

Literature study showed that morphology was studied based on the variations carried out in a particular preparation method only like concentration of monomer, dopant, oxidant, solvent and other reaction conditions viz. temperature [31–34]. However, no reports are available on the polymerization carried out by different methods and comparison of their structural variation. Since morphology is an important aspect, therefore in this communication ppy was prepared by four different polymerization techniques viz. electrochemical polymerization (EP), interfacial polymerization (IP), chemical oxidative polymerization (COP) and template-assisted polymerization (TAP) to study and explain the change in morphology obtained by SEM and high-resolution transmission electron microscopy (HRTEM). Further, the effect of morphology on redox and structural properties was interpreted and the applicability of ppy as a Pb^{2+} sensor was also checked.

2 Experimental

2.1 Materials and methods

Pyrrole monomer (99%, Spectrochem) was distilled prior to use, cyclohexane (Spectrochem), ammoniumpersulfate, $(\text{NH}_4)_2\text{S}_2\text{O}_8$ (APS) (CDH), phosphate buffered saline (PBS) tablets (Sigma-Aldrich), cetyltrimethylammonium bromide (CTAB, Spectrochem), potassium ferrocyanide, $\text{K}_4\text{Fe}(\text{CN})_6 \cdot 3\text{H}_2\text{O}$ (CDH), potassium ferricyanide, $\text{K}_3\text{Fe}(\text{CN})_6$ (SRL), lead(II) acetate trihydrate, $\text{Pb}(\text{CH}_3\text{COO})_2 \cdot 3\text{H}_2\text{O}$ (CDH), sodium acetate trihydrate, $\text{CH}_3\text{COONa} \cdot 3\text{H}_2\text{O}$ (Fisher Scientific), acetic acid glacial, CH_3COOH (SRL) were of AR grade and used as such. Nafion D-520 dispersion (5% w/w in water and 1-propanol, Alfa Aesar) and ethanol were also used as such and deionized water was used for all experiments. 10 mM stock solution of Pb^{2+} was used for making further dilutions.

2.2 Apparatus

The morphological studies were evaluated using scanning electron microscopy (SEM) on SEM ZEISS EVO18 at a voltage of 20 kV and HRTEM on FEI Tecnai G2 F30 at 300 kV. HRTEM samples were prepared by dropping 2 μL of their ethanolic dispersions made by ultrasonication (40 kHz) on to carbon coated copper grids. Fourier transform infrared (FT-IR) spectra were recorded using Shimadzu IRAffinity-1S in KBr pellet mode with 45 scans at a resolution of 4 cm^{-1} from 4000 to 400 cm^{-1} . UV–Vis spectra were measured on a Hitachi U-2900 UV–Vis spectrophotometer. X-ray diffraction (XRD) data were collected on a Rigaku Ultima IV X-ray diffractometer with $\text{Cu K}\alpha$ radiation ($\lambda = 1.541 \text{ \AA}$) at an operating voltage and

current of 40 kV and 30 mA respectively. Electrochemical experiments viz. Cyclic Voltammetry and Differential Pulse Voltammetry (DPV) were carried out in a conventional three electrode cell connected to a potentiostat (CorrTest two channel electrochemical workstation). The working electrode was bare indium tin oxide (ITO) coated glass slides (1 $\text{cm} \times 3 \text{ cm}$) or modified ITO, while platinum wire and Ag/AgCl (3 M KCl) electrode served as the counter and reference electrodes respectively. ITO was cleaned by ultrasonication in soap solution, deionized water and acetone prior to use.

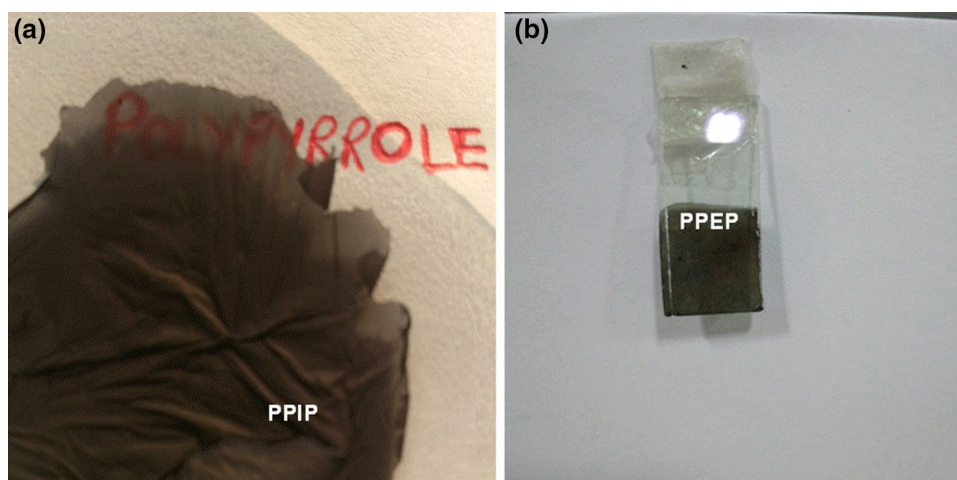
2.3 Preparation of polypyrrole by chemical oxidative polymerization (PPCP)

Ethanolic solution of pyrrole (50 mM, 20 mL) was taken in a round bottom flask and to the above solution under constant stirring; APS (12.5 mM) was added over a period of 30 min. The polymerization was allowed to occur for 24 h. Thus the final [oxidant]/[monomer] ratio was 0.25. On completion of 24 h the product was collected by centrifuging the solution which was sequentially washed first with deionized water and then ethanol to remove the unreacted APS and monomer, if any. The washed product was dried at 60 $^\circ\text{C}$ in an oven overnight and was stored in a desiccator.

2.4 Preparation of polypyrrole by interfacial polymerization (PPIP)

A similar procedure as reported earlier was used [35] with slight modifications. An aqueous solution of APS (12.5 mM, 20 mL) was poured in a petri dish of 13.5 cm diameter and cooled to 8–10 $^\circ\text{C}$. It was followed by slow addition of a pre cooled solution of pyrrole (50 mM, 20 mL) at the same temperature, prepared in cyclohexane (organic phase) from the sides on top of aqueous phase. It resulted in the formation of interface by two immiscible phases. Thereafter, the petri dish was kept undisturbed at 8–10 $^\circ\text{C}$ for 24 h and ppy film formed at the interface. Cyclohexane solution was carefully removed from the petri dish that exposed a black colored ppy film on top of aqueous phase. To remove the aqueous phase, the petri dish was slightly tilted due to which the film got detached from one side and hence aqueous phase was easily decanted from the bottom. Thus, only the film remained in the container which was washed with deionized water and ethanol. The film was dried at 60 $^\circ\text{C}$ in an oven. A digital photograph of the film (PPIP) is given in Fig. 1a. The [oxidant] / [monomer] and the time of reaction were optimized by changing the molar ratio as 0.025, 0.25 and 1.25 and the time duration as 6, 24 and 48 h.

Fig. 1 Digital photograph of **a** PPIP and **b** ITO with PPEP



2.5 Preparation of polypyrrole nanofibers (PNF)

PNF were prepared using the method reported by Zhang et al. [36]. Pyrrole monomer (0.03 M) was added to a homogeneous aqueous solution of cationic surfactant, CTAB (30 ml, 0.01 M) and was stirred for 10 min. It was cooled to around 5–8 °C. A pre-cooled solution of APS (0.14 M, 6.5 mL) was added to it drop-wise with stirring. It resulted in the formation of a white precipitate which turned to black color. The reaction mixture was kept at 0 °C for 24 h followed by centrifugation, washing with deionized water and ethanol. The obtained PNF were dried at 60 °C overnight.

2.6 Preparation of polypyrrole by electrochemical polymerization (PPEP)

This was carried out using cyclic voltammetry with a pre-cleaned ITO as the working electrode in the three electrode electrochemical cell. Pyrrole solution (50 mM, 40 mL) prepared in PBS (0.01M, pH 7) was used as the monomer solution as well as the electrolyte. It was subjected to a sweeping potential of 0–1.1 V for 25 complete cycles at a scan rate of 0.050 V s⁻¹ resulting in black colored ppy film on ITO. The film was washed with PBS and deionized water and was air dried. A digital photograph of ITO with PPEP film is given in Fig. 1b.

2.7 Electrode fabrication and electrochemical testing

The working electrodes except PPEP were fabricated by drop casting 20 μL of the homogeneous mixture made by ultrasonating the sample (5 mg), Nafion (5 μL) and isopropanol on pre-cleaned ITO which were designated as PPCP, PPIP and PNF electrodes. The detection of Pb²⁺ (10 μM) by PNF, PPCP, PPIP and PPEP electrodes was inspected using DPV in 0.1 M acetic acid-sodium acetate buffer (HAc-NaAc, pH 5.3) from -1.0 to 0.5 V with increment potential

of 0.004 V, pulse amplitude of 0.050 V, pulse width of 0.03 s and pulse period of 0.2 s while the electrochemical property of the above electrodes was examined by cyclic voltammetry in 1 mM Fe(CN)₆^{4-/3-} with 0.1 M KCl as the supporting electrolyte in a potential window of -0.6 to +0.6 V and a scan rate of 0.025 V s⁻¹.

3 Results and discussions

3.1 FT-IR spectroscopy

The FT-IR spectra of PPCP, PPIP, PPEP and PNF are represented by Fig. 2. It was clear that successful polymerization of pyrrole to ppy had occurred, as all the characteristic bands were present according to reported literature [36–38]. The broad band around 3000–3500 cm⁻¹ was ascribed to N–H and aromatic C–H stretching vibrations. The peaks around 1548 and 1479 cm⁻¹ described the antisymmetric and symmetric ring stretching modes of polypyrrole respectively however for PPEP, overoxidized ppy was present as elucidated by the appearance of peak at 1635 cm⁻¹ attributed to C=O in pyrrolidone. Peaks around 1313 and 1043 cm⁻¹ were attributed to C–N stretching and C–H in-plane deformation vibration denoting 2,5-disubstituted pyrrole respectively. Furthermore, the two peaks at ~1192 and ~914 cm⁻¹ represented the doping state of polypyrrole. As seen for PPEP the latter peak was very weak. The bands at ~964 and ~786 cm⁻¹ established the formation of polymerized pyrrole corresponding to C–C and C–H out-of-plane ring deformation respectively.

3.2 Optical studies by UV–Vis spectroscopy

The UV–Vis absorption spectra of PPCP, PPIP, PPEP and PNF are shown in Fig. 3. The absorption spectra of PPCP, PPIP, PPEP and PNF depicted the presence of a band

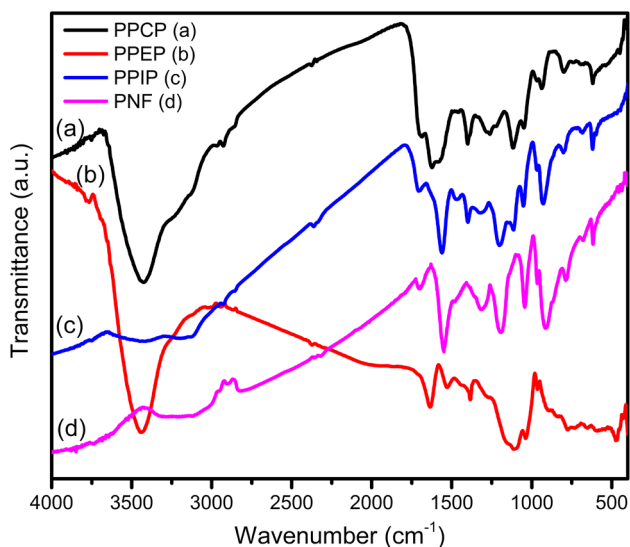


Fig. 2 FT-IR spectra of *a* PPCP (black), *b* PPEP (red), *c* PPIP (blue) and *d* PNF (pink)

between 400 and 500 nm which was attributed to $\pi \rightarrow \pi^*$ transition of ppy chains signifying conjugation as it was red shifted vis-à-vis pyrrole monomer, which has a peak $\sim 200\text{--}250$ nm [39]. The broad absorption band beyond 600 nm in the case of PPCP, PPIP and PNF denoted the transitions from the valence (π) band to polaron/bipolaron/antibonding bipolaron band [40, 41], hence existing in their doped forms however for PPEP this transition was absent due to its overoxidized and insulating nature as also found out by FT-IR analysis.

3.3 X-ray diffraction studies

The X-ray diffractograms depicted in Fig. 4 showed that PPCP, PPIP, PPEP and PNF all have poor crystallinity and amorphous nature which is a characteristic feature of ppy [42]. PPCP, PPIP and PNF had broad peaks centered at $2\theta = 24.3^\circ$, 25.4° and 23.6° with d-spacing of 3.66, 3.50 and 3.77 Å respectively which are assigned to face-to-face stacking of pyrrole rings [42, 43]. On the other hand, for PPEP,

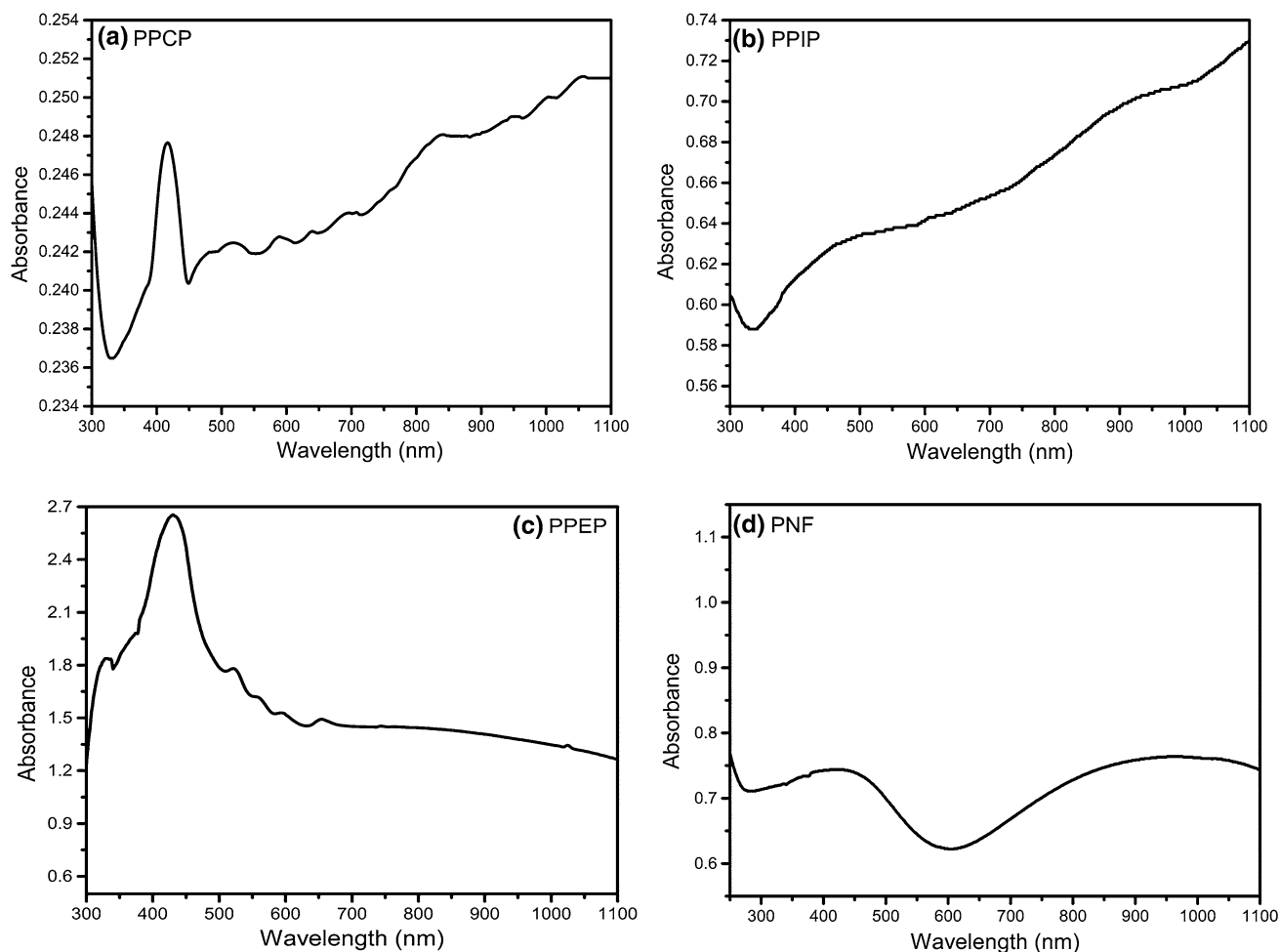


Fig. 3 UV-Vis absorption spectra of *a* PPCP, *b* PPIP, *c* PPEP and *d* PNF

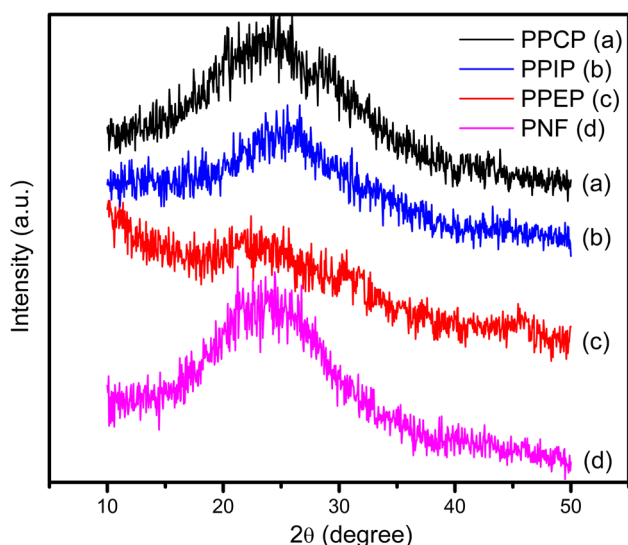


Fig. 4 XRD pattern of *a* PPCP (black), *b* PPIP (blue), *c* PPEP (red) and *d* PNF (pink)

it extended in the 2θ region of 20° – 30° . The resulting peaks were due to the scattering from ppy chains at interplanar distance. It was observed from the X-ray diffractograms that PPEP had a lower degree of order as compared to other three forms which could be attributed to carbonyl group in the polymer backbone responsible for distorting its orientation.

3.4 Morphological studies and formation mechanism

Morphological analysis by SEM depicted that completely different structures of PPIP, PPCP, PPEP and PNF were obtained by the four methods employed viz. interfacial (Figs. 5, 6a, b), chemical oxidative (Fig. 7a, b), electrochemical (Fig. 7c, d) and template-assisted polymerization (Fig. 7e). The observed different morphologies of PPIP, PPCP and PPEP were explained on the basis of rate of polymerization and the dimension of the space available for polymerization to take place. In interfacial polymerization, the [oxidant]/[monomer] and the time of reaction were also

Fig. 5 SEM micrographs of PPIP *a, b* organic phase side and *c, d* aqueous phase side

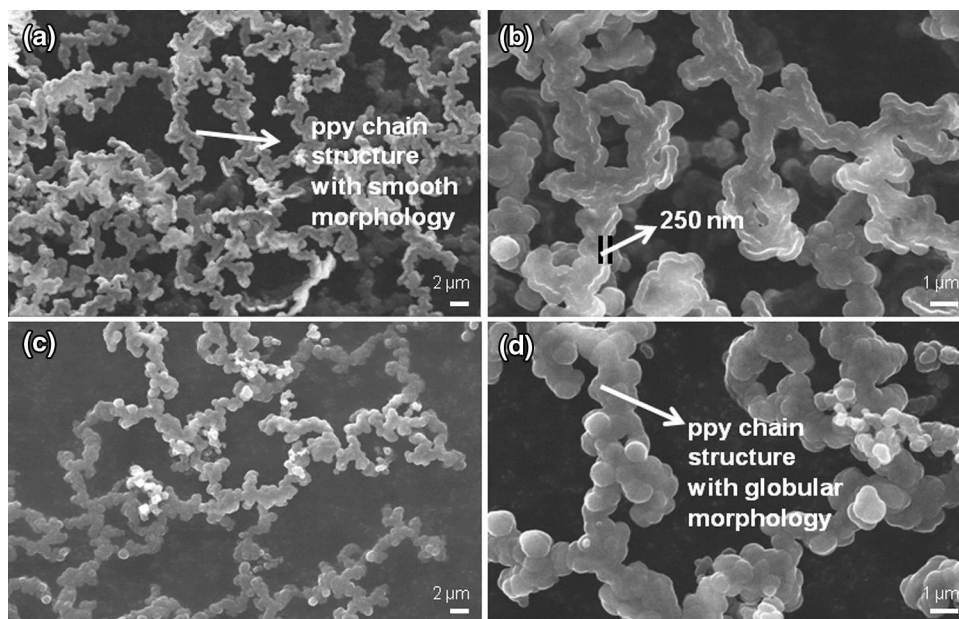
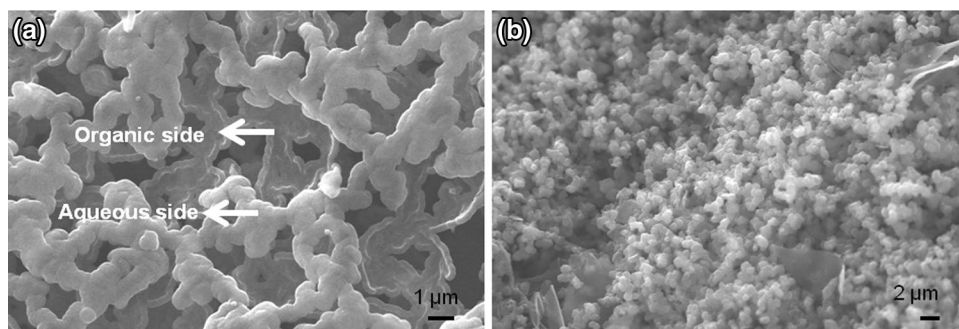


Fig. 6 SEM images of *a* PPIP showing both the organic and aqueous side for comparison and *b* ppy collected from the bottom of the petri dish in case of interfacial polymerization



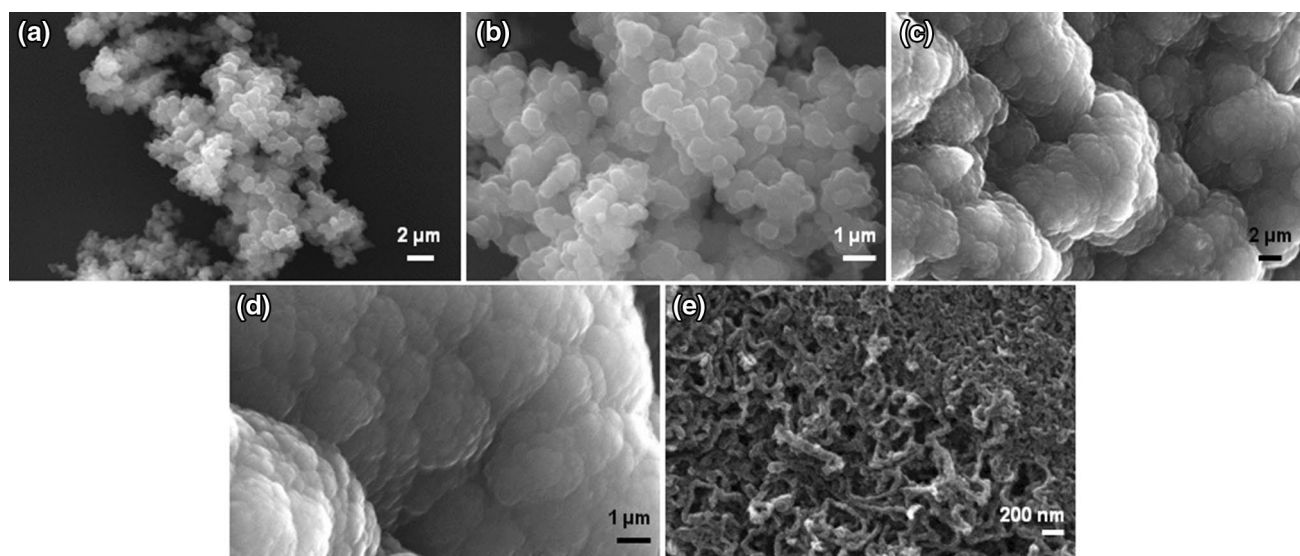


Fig. 7 SEM micrographs of **a, b** PPCP, **c, d** PPEP and **e** PNF

varied. The molar ratio was taken as 0.025, 0.25 and 1.25 whereas the effect of time duration was examined over a period of 6, 24 and 48 h. At 0.025 molar ratio, irregular spherical morphology of ppy was detected without much change in the size of the spheres that ranged from 200 to 260 nm with increase in time duration. The molar ratio of 0.25 resulted into chain like morphology of ppy at 24 and 48 h, however at 6 h, chain and spheres both formed and with increase of time period the thickness of the chains increased to ~340 nm from ~250 nm. At 1.25 molar ratio, ppy again took the shape of chains but were quite thick, and longer duration caused them to become thicker extending from 0.5 to ~1 μm which could lead to lower surface area and inferior electrochemical properties. Thus, 0.25 and 24 h were the optimized molar ratio and time duration for polymerization as regular structure was obtained. Interfacial polymerization occurred through a diffusion controlled process in which APS from the aqueous phase and pyrrole from the organic phase (cyclohexane) both diffused towards the interface. As a result, the constituents met only at the interface in a limited amount as [oxidant]/[monomer] ratio was kept low and the reaction temperature was also low. Thus, the reaction conditions that prevailed made the rate of polymerization slow. Furthermore, the interface provided a two dimensional space for ppy to grow, therefore it formed as a film, with varying morphologies on aqueous and organic phase sides. A network of chain like morphology was found on both sides but the texture was completely different. On the organic phase side very smooth morphology was observed whereas on the aqueous side it had globular morphology, a clear comparison was seen in Fig. 6a. It was described as follows; since cyclohexane is lighter than water it formed the top layer

in which pyrrole was dissolved. As it diffused towards the interface, it was slightly pulled downwards by gravitational force and developed into droplets; followed by reaction with APS thus ppy achieved spherical globular morphology on the aqueous side and smooth surface with concave circular grooves on the organic phase side. The role of dimension of the polymerization space was justified by the fact that ppy collected from the bottom of the petri dish in interfacial polymerization, did not have the same morphology as obtained for the film formed at the interface. It was in the shape of spheres (Fig. 6b). This changed morphology was accounted by the three dimensional space which the bulk of the aqueous phase provided, for ppy to grow in all directions. The polymer reached at the base of the petri dish because in the initial stages of interfacial polymerization black drops of polymer were seen travelling towards the bottom of the aqueous layer from the interface; probably because pyrrole was soluble in water also and the oligomers created in the beginning were dispersible in water. With the progress of polymerization the aqueous layer turned black and further movement of polymer towards aqueous layer was hindered as a film developed at the interface.

In chemical oxidative polymerization (Fig. 7a, b), inter-linked microspheres of 200–250 nm size were created which were not aggregated as the rate of polymerization was again kept low by maintaining a small [oxidant]/[monomer] ratio and the addition of oxidant (APS) was done over a long period of time. Moreover, due to the accessibility of three dimensional spaces in the bulk of the reaction mixture it acquired spherical morphology.

Electrochemical polymerization (Fig. 7c, d), was characterized by rapid oxidation of pyrrole monomers that led to

uncontrolled polymer growth resulting in globular aggregated cauliflower structures. The product ppy formed as a film adhered to the surface of the working electrode whereby after the formation of initial layer of polymer on the surface, it kept on growing on top of it increasing the thickness of the film with time.

Polypyrrole nanofibers (PNF) were prepared using a self degrading oxidative template comprising of CTAB and APS which resulted in the formation of fibrous morphology as shown in Fig. 7e. The diameters of the nanofibers formed were of the range 29–57 nm. On addition of pyrrole monomers they positioned into the hydrophobic cavity of the micelles formed by CTAB aqueous solution which was at a higher concentration than its critical micelle concentration (CMC) (0.91 mM) [44]. Thereafter, APS formed a white precipitate of $(CTA)_2S_2O_8$. This led to the formation of lamellar micelles and lamellar polypyrrole were prepared but with the reduction of persulfate ions being used during polymerization led to the weakening of the lamellae structures causing an increase in the surface/interface energy. This resulted in rolling of the lamellae to lower the energy [45] leading to the formation of PNF.

HRTEM images of PPIP (Fig. 8a) and PPCP (Fig. 8b) were consistent with that of SEM morphology representing chain and interlinked microspheres respectively.

3.5 Electrochemical characterization and Pb^{2+} detection

The electrochemical activity of PPCP, PPIP, PPEP and PNF electrodes was examined by cyclic voltammetry technique. A comparison of their cyclic voltammograms (CVs) is given in Fig. 9. CVs of PPCP, PPIP and PNF depicted the presence of conspicuous redox peaks attributed to the $Fe(CN)_6^{4-/3-}$ redox couple inferring that the surfaces were electroactive and conductive. It was noticed that they represented quasi-reversible nature with anodic and cathodic peak

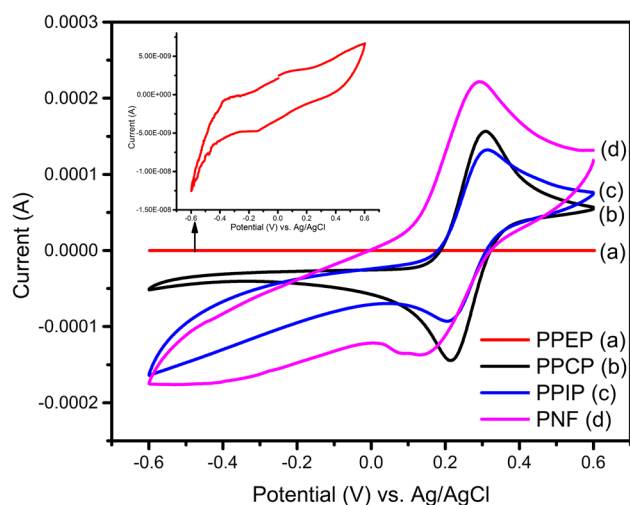
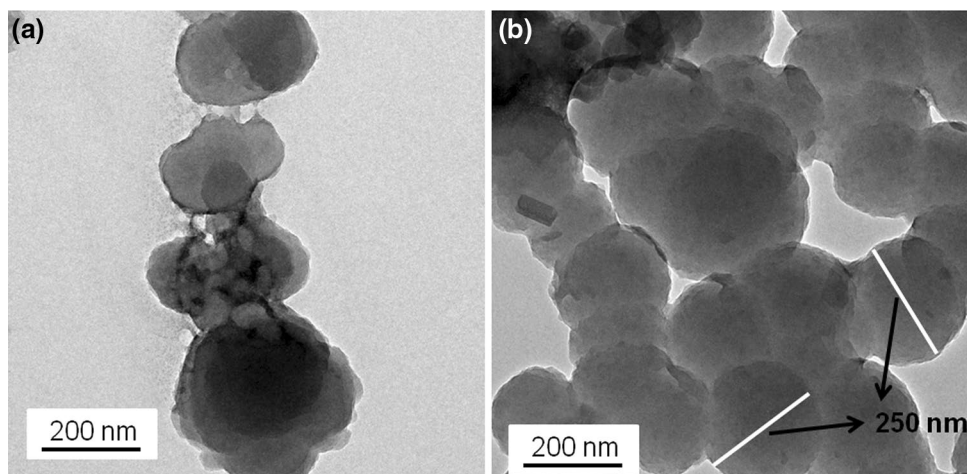


Fig. 9 Cyclic Voltammograms of *a* PPEP (red), *b* PPCP (black), *c* PPIP (blue) and *d* PNF (pink) in 1 mM $Fe(CN)_6^{4-/3-}$ with 0.1 M KCl as the supporting electrolyte over a potential window of -0.6 to $+0.6$ V at a scan rate of 0.025 V s^{-1} (inset is the magnified version of *a* PPEP)

potential difference ($E_p^a - E_p^c = \Delta E_p$) and peak current ratio, $|I_p^a/I_p^c|$ as 90 mV, 1.09 for PPCP, 98 mV, 1.39 for PPIP and 149 mV, 1.84 for PNF thus signifying diffusion controlled process. The overall electrochemical performance of PPEP was the lowest among the three with reduced current and weak redox peaks that suggested the deteriorated polymer backbone due to presence of carbonyl group of pyrrolidone moiety causing hindrance in charge transfer across the electrode [22]. Since PPEP was synthesized using PBS, pH 7, it resulted in overoxidation and insulated ppy [46]. FT-IR and UV-Vis analysis also corroborated the same for PPEP. Therefore, the effect of morphology on the electrochemical performance was clearly visible as PPEP which had irregular aggregated cauliflower structure prevented the diffusion of

Fig. 8 HRTEM images of *a* PPIP and *b* PPCP



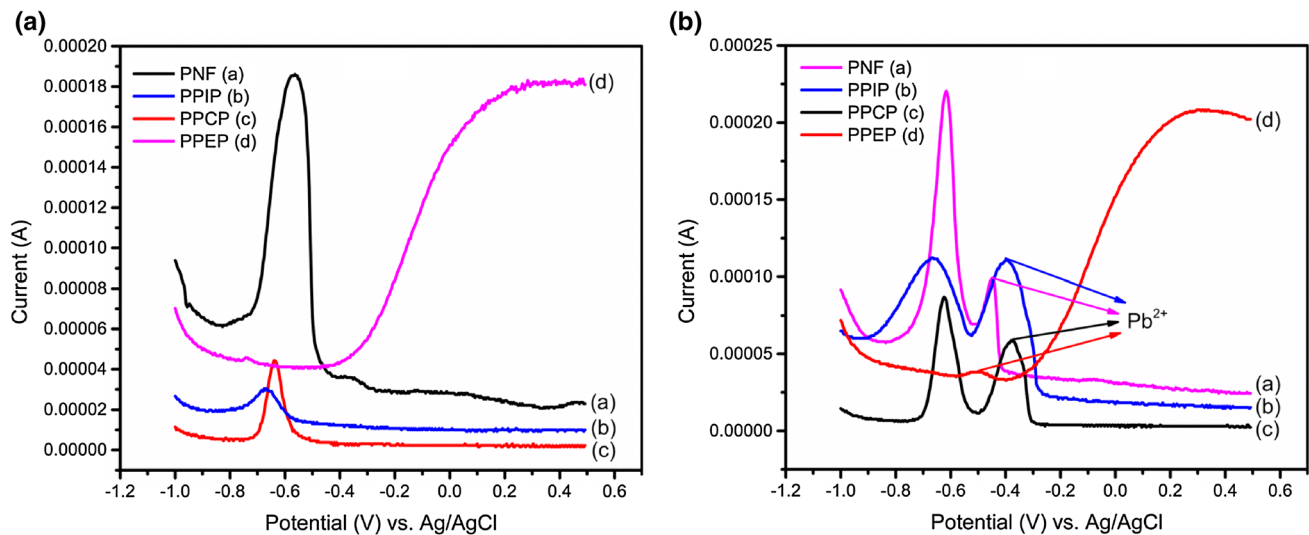


Fig. 10 Differential Pulse Voltammograms of PNF, PPIP, PPCP and PPEP in **a** absence of Pb^{2+} and **b** presence of Pb^{2+} ($10 \mu\text{M}$) in 0.1 M HAc-NaAc , pH 5.3 from -1.0 to 0.5 V with increment potential of

0.004 V , pulse amplitude of 0.050 V , pulse width of 0.03 s and pulse period of 0.2 s

ions and thus slowed the electrode reactions. On the other hand, PPCP, PPIP and PNF with a relatively regular morphology of interconnected spheres, chain and nanofibers structure respectively with smaller size than PPEP provided an increased surface area and better channel for ion diffusion, thus making the process faster and effective [24]. PNF with the highest surface-to-volume ratio recorded the largest current due to its enhanced electroactive surface area. Also, from the CVs of PPIP and PNF it was deduced that they showed pseudocapacitive property. Thus, it was observed that ordered architecture of PPIP and PNF made charge storage possible by fast Faradaic reactions [47].

Pb^{2+} detection by PPCP, PPIP, PPEP and PNF electrodes was checked by DPV in 0.1 M HAc-NaAc , pH 5.3. The influence of pH was investigated in a range of 3.6–5.8 and the optimum pH was found out to be 5.3 which was due to the fact that at lower pH values, H^+ was the competing factor with the metal ion and higher pH could lead to the hydrolysis of metal ion. The voltammograms recorded in the absence and presence of Pb^{2+} ($10 \mu\text{M}$) are shown in Fig. 10. It was noticed that in comparison with the blank, peaks corresponding to Pb^{2+} were visible in all the cases at -0.45 , -0.39 , -0.37 and -0.50 V for PNF, PPIP, PPCP and PPEP electrodes respectively, which was attributed to the interaction of the metal ion with the lone pair of electrons present on Nitrogen of ppy. The other peak at around -0.6 and -0.67 V for PNF, PPCP and PPIP was due to polypyrrole. It was absent in PPEP, that again depicted its overoxidized nature. Also, PPEP vis-à-vis other electrodes, represented a less defined peak for Pb^{2+} at more negative potential, suggesting the feasibility of other electrode surfaces for Pb^{2+} detection.

4 Conclusions

Polypyrrole was successfully prepared by four different polymerization techniques which was confirmed by FT-IR, UV-Vis and XRD analytical techniques. The effect on morphology was clearly visible which varied from chains, microspheres and nanofibers in interfacial, chemical oxidative polymerization and template-assisted polymerization to cauliflower like structures produced by electrochemical process. It was observed that ordered structures had better structural and electrochemical properties than irregular morphology with PPEP being the least ordered among PPCP, PPIP and PNF. Furthermore, from the CV curves it was noticed that PPIP and PNF showed pseudocapacitive behavior and DPV technique established Pb^{2+} sensing capability of all ppys.

Acknowledgements The author (Shruti Peshoria) would like to express gratitude to Guru Gobind Singh Indraprastha University for providing financial support in terms of Indraprastha Research Fellowship (IPRF) with award number GGSIPU/DRC/Ph.D/Adm./2014/1634 and Ms. Neeru Sharma for administrative services. Also, the authors would like to thank Jamia Millia Islamia, New Delhi for HRTEM facility.

References

1. H. Shirakawa, E.J. Louis, A.G. MacDiarmid, C.K. Chiang, A.J. Heeger, *J. Chem. Soc., Chem. Commun.* **578** (1977)
2. A.G. MacDiarmid, *Synth. Met.* **125**, 11 (2001)
3. A.T. Mane, S.D. Sartale, V.B. Patil, *J. Mater. Sci.: Mater. Electron.* **26**, 8497 (2015)

4. S. Liu, Y. Ma, R. Zhang, X. Luo, *ChemElectroChem* **3**, 1799 (2016)
5. B.V. Chaluvvaraju, S.K. Ganiger, M.V. Murugendrappa, *J. Mater. Sci.: Mater. Electron.* **27**, 1044 (2016)
6. Q. Zhou, G. Shi, *J. Am. Chem. Soc.* **138**, 2868 (2016)
7. C. Chang, X. Yang, S. Xiang, H. Que, M. Li, *J. Mater. Sci.: Mater. Electron.* **28**, 1777 (2017)
8. V.K. Thakur, M.R. Kessler, in *Advanced Energy Materials*, ed. by A. Tiwari, S. Valyukh. *Polymer Nanocomposites: New Advanced Dielectric Materials for Energy Storage Applications* (John Wiley & Sons, Inc., Hoboken, NJ, 2014), p. 207
9. M.S. Rahman, W.A. Hamed, R.B. Yahya, H. N. M. Ekramul Mahmud, *J. Polym. Res.* **23**, 192 (2016)
10. J. Huo, M. Zheng, Y. Tu, J. Wu, *J. Mater. Sci.: Mater. Electron.* **27**, 5680 (2016)
11. C. Bora, S.K. Dolui, *Polymer* **53**, 923 (2012)
12. Z. Zha, Z. Deng, Y. Li, C. Li, J. Wang, S. Wang, E. Qu, Z. Dai, *Nanoscale* **5**, 4462 (2013)
13. P.K. Kalambate, R.A. Dar, S.P. Karna, A.K. Srivastava, *J. Power Sources* **276**, 262 (2015)
14. K. Saranya, Md. Rameez, A. Subramania, *Eur. Polym. J.* **66**, 207 (2015)
15. P. Xu, X. Han, B. Zhang, N.H. Mack, S.-H. Jeon, H.-L. Wang, *Polymer* **50**, 2624 (2009)
16. P.-C. Wang, R.E. Lakis, A.G. MacDiarmid, *Thin Solid Films* **516**, 2341 (2008)
17. J. Hazarika, A. Kumar, *J. Polym. Res.* **23**, 95 (2016)
18. F.A.G. da Silva Jr., J.C. Queiroz, E.R. Macedo, A.W.C. Fernandes, N.B. Freire, M.M. da Costa, H.P. de Oliveira, *Mater. Sci. Eng. C* **62**, 317 (2016)
19. I. Sapurina, J. Stejskal, I. Šeděnková, M. Trchová, J. Kovářová, J. Hromádková, J. Kopecká, M. Cieslar, A.A. El-Nasr, M.M. Ayad, *Synth. Met.* **214**, 14 (2016)
20. A. Morozan, P. Jégou, S. Campidelli, Serge Palacin, B. Jusselme, *Chem. Commun.* **48**, 4627 (2012)
21. S. Carquigny, O. Segut, B. Lakard, F. Lallemand, P. Fievet, *Synth. Met.* **158**, 453 (2008)
22. J.K. Gan, Y.S. Lim, N.M. Huang, H.N. Lim, *Appl. Surf. Sci.* **357**, 479 (2015)
23. J. Zhu, Y. Xu, J. Wang, J. Wang, Y. Bai, X. Du, *Phys. Chem. Chem. Phys.* **17**, 19885 (2015)
24. R. Wannapob, M.Y. Vagin, I. Jeerapan, W.C. Mak, *Langmuir* **31**, 11904 (2015)
25. L. Liang, G. Chen, C.-Y. Guo, *Compos. Sci. Technol.* **129**, 130 (2016)
26. L.-Y. Chang, C.-T. Li, Y.-Y. Li, C.-P. Lee, M.-H. Yeh, K.-C. Ho, J.-J. Lin, *Electrochim. Acta* **155**, 263 (2015)
27. Y. Tian, J. Zhang, S. Tang, L. Zhou, W. Yang, *Small* **12**, 721 (2016)
28. K. Ghanbari, N. Hajheidari, *J. Polym. Res.* **22**, 152 (2015)
29. H.G. Lemos, S.F. Santos, E.C. Venancio, *Synth. Met.* **203**, 22 (2015)
30. L. Tian, Y. Feng, Y. Qi, B. Wang, X. Fu, Y. Chen, *J. Polym. Res.* **18**, 2379 (2011)
31. C. He, C. Yang, Y. Li, *Synth. Met.* **139**, 539 (2003)
32. G.T. -Gómez, P.G. -Romero, *Synth. Met.* **98**, 95 (1998)
33. N.H.A. Rahman, T.I.T. Kudin, A.M.M. Ali, M.Z.A. Yahya, *J. Mater. Sci. Eng. A* **2**, 190 (2012)
34. R.A.M. Campos, V.A. Silva, R. Faez, M.C. Rezende, *Polímeros* **26**, 197 (2016)
35. G. Qi, Z. Wu, H. Wang, *J. Mater. Chem. C* **1**, 7102 (2013)
36. X. Zhang, J. Zhang, Z. Liu, C. Robinson, *Chem. Commun.* **16**, 1852 (2004)
37. Y. Cai, Z. Qin, L. Chen, *Prog. Nat. Sci.: Mater. Int.* **21**, 460 (2011)
38. A. Dagar, A.K. Narula, *J. Mater. Sci.: Mater. Electron.* **28**, 8643 (2017)
39. H. Peng, C. Soeller, N.A. Vigar, V. Caprio, J. Travas-Sejdic, *Biosens. Bioelectron.* **22**, 1868 (2007)
40. A. Singh, Z. Salmi, P. Jha, N. Joshi, A. Kumar, P. Decorse, H. Lecoq, S. Lau-Truong, D.K. Aswal, S.K. Gupta, M.M. Chehimi, *RSC Adv.* **3**, 13329 (2013)
41. X. Wang, T. Wang, D. Liu, J. Guo, P. Liu, *Ind. Eng. Chem. Res.* **55**, 866 (2016)
42. Y. Fu, Y.S. Su, A. Manthiram, *J. Electrochem. Soc.* **159**, A1420 (2012)
43. A. Liu, C. Li, H. Bai, G. Shi, *J. Phys. Chem. C* **114**, 22783 (2010)
44. T. Carmona, M. Pineiro, C.J.P. Monteiro, M.M. Pereira, A.J.M. Valente, *Colloids Surf. A* **481**, 288 (2015)
45. L.Y. Shi, J.Q. Wang, L. Gao, L. Huang, J. Zhu, Y. Wang, X. Fan, T. Yu, M. Zhu, Z. Li, Z. Zou, *Mater. Manuf. Processes* **22**, 705 (2007)
46. C. Debiemme-Chouvy, *Electrochem. Solid-State Lett.* **10**, E24 (2007)
47. Z.-H. Huang, Y. Song, X.-X. Xu, X.-X. Liu, *ACS Appl. Mater. Interfaces* **7**, 25506 (2015)